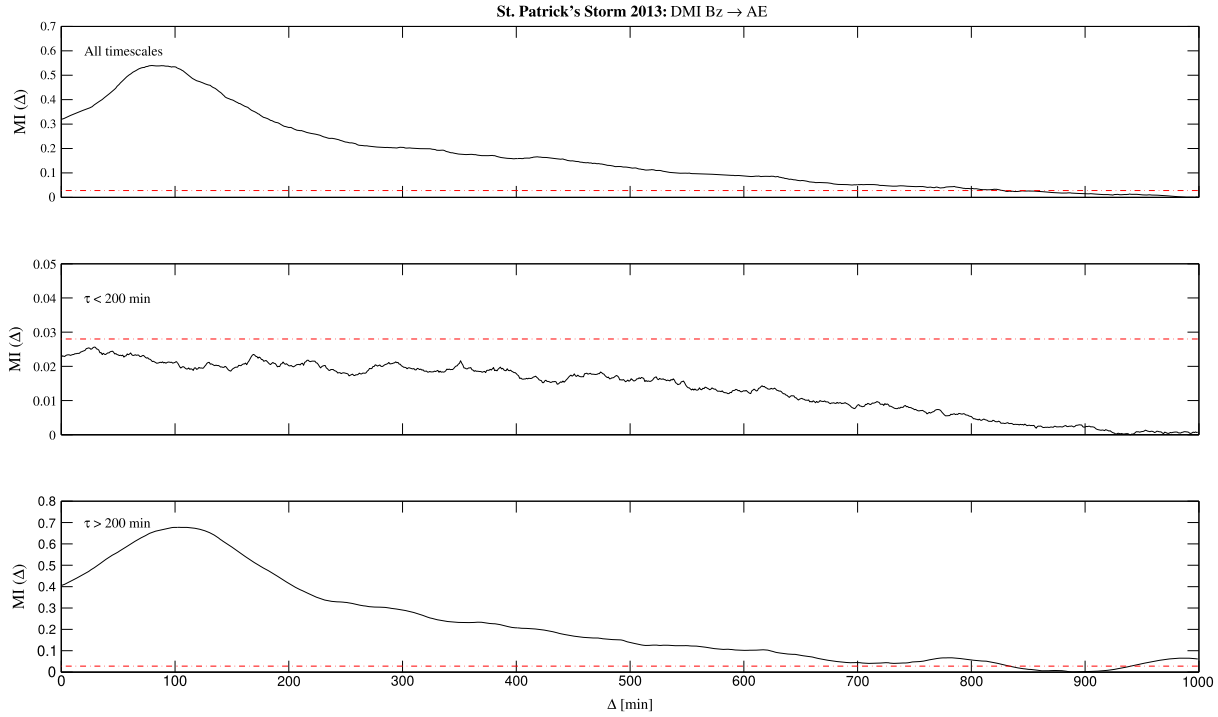

Figure 8. The DMI analysis between IMFs of the interplanetary magnetic field B_z component and auroral electroject *AE* index for (top) the actual, (middle) the short-timescale ($\tau < 200$ min), and (bottom) the long-timescale ($\tau > 200$ min) signals for the 2013 St. Patrick's storm time period. The dashed red line is the significance (5% null hypothesis) DMI threshold, $MI_{thr} = 0.028$.

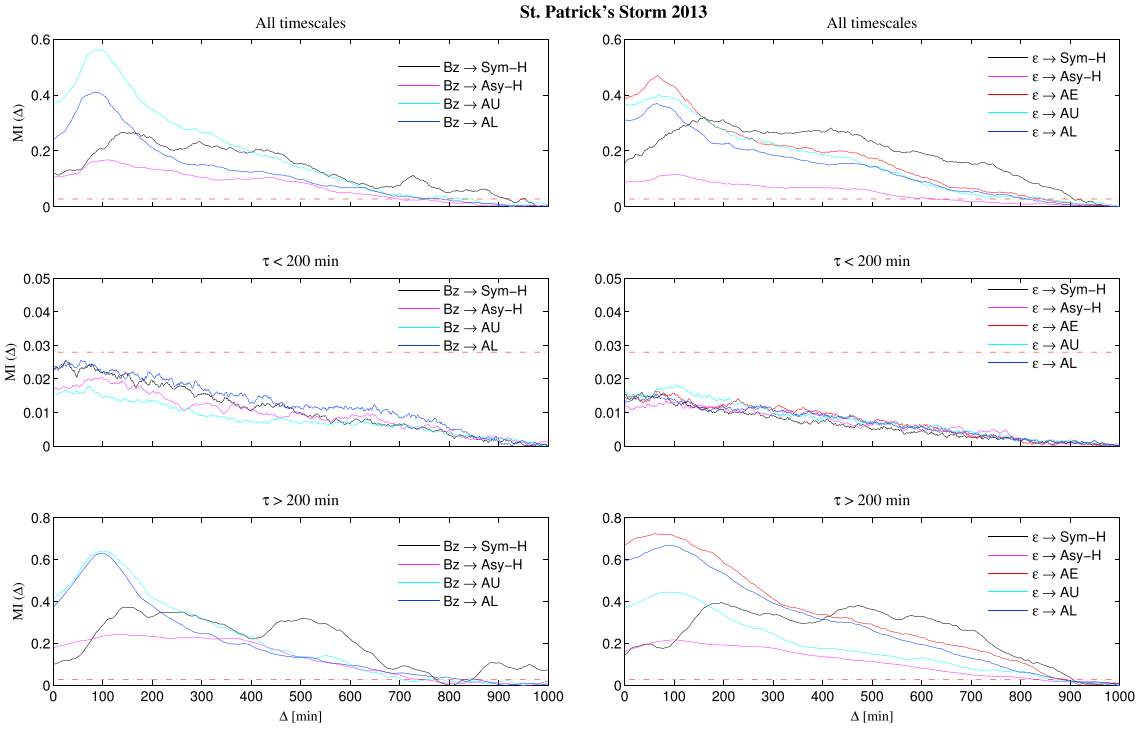

Figure 9. The DMI results on different timescales between solar wind IMF B_z component, the Perrault-Akasofu coupling function, ϵ, and magnetospheric response proxies, *SYM-H*, *ASY-H*, *AE*, *AU*, and *AL*, for the 2013 St. Patrick's storm time period. The dashed red line represents the significance (5% null hypothesis) DMI threshold, $MI_{thr} = 0.028$.

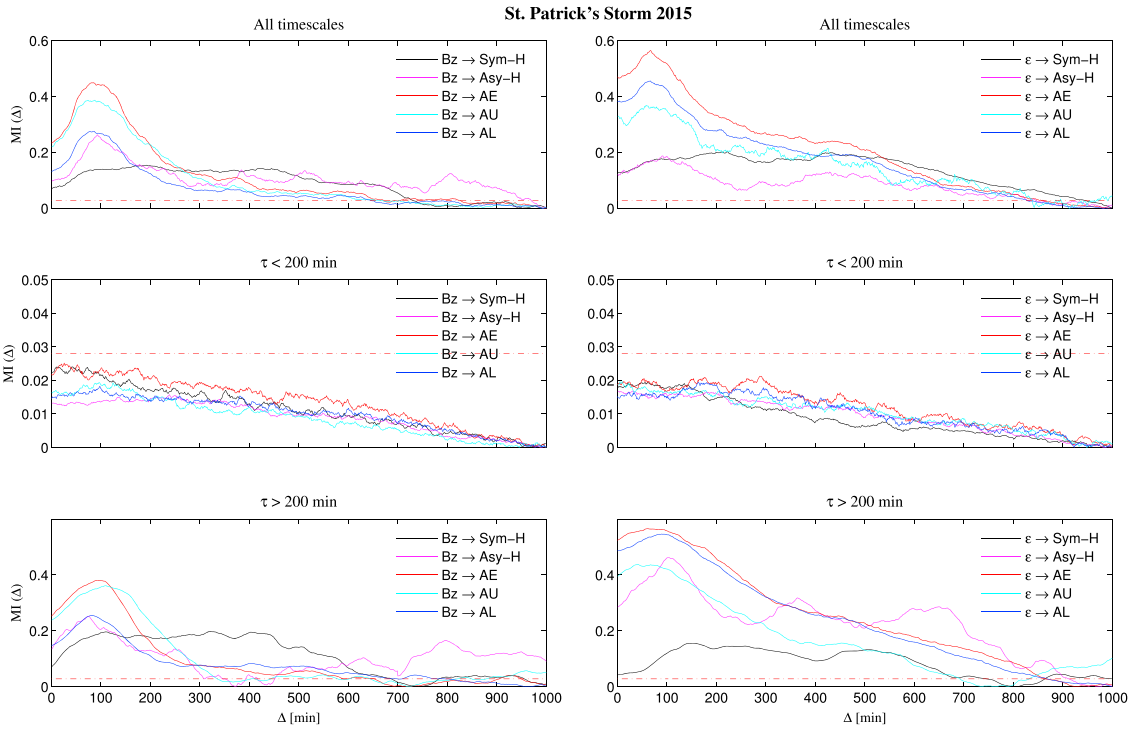

Figure 10. As in Figure 9 for the 2015 St. Patrick's storm time period.

coupled to (driven by) solar wind, while for timescales shorter than 200 min, there is no direct coupling to solar wind parameter fluctuations. The same results are found in the case of the 2015 St. Patrick's Day storm as shown in Figure 10.

Another interesting feature emerging from our analysis is how at long timescales the response of the magnetospheric ring current, as monitored by *SYM-H*, is delayed with respect to the high-latitude electrojet current systems. Indeed, while for high-latitude geomagnetic indices (*AE*, *AU*, and *AL*) the maximum of the MI(Δ) is found in correspondence of Δ ∼ 100 min (Δ ∼ 70–80 min for ACE-propagated data), *SYM-H* responds later being Δ ∼ 150–200 min (Δ ∼ 100–150 min for ACE-propagated data). A more different behavior is shown by *ASY-H*, which indeed shows a maximum of the MI(Δ) for a time delay of Δ ∼ 100 min (Δ ∼ 60–80 min for ACE-propagated data), i.e., a time delay similar to the high-latitude geomagnetic indices. This result confirms the previous findings by *Crooker* [1972] and *Clauer and McPherron* [1980] that showed that the asymmetric part of the variation of the horizontal component *H* of geomagnetic field at low latitude well correlates with the general trend of the auroral electrojet index *AE*. Furthermore, the time delay corresponding to the DMI maximum observed in the case of *AE* indices and *ASY-H* seems to be well in agreement with the time necessary to the interplanetary disturbance (CME) to propagate from L1 (ACE) to the magnetopause plus the typical ∼64–72 min of the median growth-phase period of southward IMF preceding a classical substorm [see, e.g., *Lyons et al.*, 1997]. The explanation of this point has to be found in the link between the development of the partial ring current and the increase of the dawn-dusk interplanetary electric field. Conversely, the possible explanation of this different response time delay observed in the case of *SYM-H* suggests that the ring current enhancement requires a longer time, this being related to the time for plasma to be convected/advected to the Earth's distances in the inner regions of the magnetosphere where the ring current is located.

Finally, the absolute and maximum values of the shared information MI at long timescales are generally higher for geomagnetic high-latitude indices (*AE*, *AU*, and *AL*) than for *SYM-H* and *ASY-H*. This suggests that there could be inner physical processes that tend to reduce the correlation between *SYM-H* and *ASY-H* and external drivers.

4. Summary and Conclusions

In this work, we have presented a detailed analysis of the response of the Earth's magnetosphere to solar wind disturbances in terms of timescale coupling during two major geomagnetic storms, the 2013 and 2015 St. Patrick's Day storms. Our analysis is based on novel approaches, the EMD and the DMI, which allow to separate fluctuations at different timescales contributing to a signal and to analyze the linear/nonlinear interference/coupling between two signals.

The main results of our work can be summarized as follows:

1. The magnetospheric short-timescale fluctuations seem to be not directly related to the same timescale fluctuations in the SW/IMF, because the MI is under the null hypothesis threshold. This is a relevant result indicating that internal magnetospheric processes strongly affect the magnetospheric response at timescales lower than 200 min in the magnetospheric dynamics. With the term "internal origin" we mean that there is not a one-to-one coupling. Anyway, the transient activities at these timescales (see, e.g., the bursty enhancement of high-latitude electrojet currents, the occurrence of fast relaxation processes in the tail regions, such as bursty bulk flows) that are responsible for the fast variations observed in the geomagnetic indices at short timescales, are certainly triggered by IMF and solar wind changes but do not seem directly driven in terms of fluctuations.
2. On the contrary, the SW/IMF fluctuations at long timescales play a primary role into the coupling of timescales greater than 200 min in the magnetosphere. This indicates that the magnetospheric response to the SW/IMF driver at these timescales is well correlated, suggesting that direct driven processes are responsible for the geomagnetic indices fluctuations at these timescales.
3. A time delay of $\Delta \sim 100-150$ min ($\Delta \sim 70-80$ min for ACE-propagated data) is found between solar wind/IMF parameters (observed at L1 position) and magnetospheric overall dynamics (measured by indices), which is quite well in agreement with the travel time necessary to the SW/IMF perturbation to propagate from the ACE spacecraft position to the Earth's magnetopause plus the response time of the Earth's magnetosphere for the occurrence of storms/substorms.
4. A great information transfer can be observed between IMF B_z component and *AE*, *AU*, and *AL* indices, while a lower transfer is found when IMF B_z component and *SYM-H*/*ASY-H* are considered.

Although in this work we have limited our discussion to the role that IMF B_z and the Perrault-Akasofu coupling function ϵ play, we remark that the same analyses have been performed to other solar wind parameters: the solar wind dynamic pressure p_{SW}, the velocity flow v, vB_{South}, and the Newell coupling function $d\Phi_{MP}/dt$ [*Newell et al.*, 2007] (not shown here). The obtained results do not show any substantial difference from those reported in this work.

Our findings support the common idea that the Earth's magnetosphere response consists of both direct driven and internal processes, where the internal processes can be considered more reasonably as only triggered by external solar wind changes. Furthermore, there is a clear separation of timescales between the internal processes and the direct driven ones, being the characteristic separation timescale of the order of 100–200 min. This timescale separation is well in agreement with previous findings on loading-unloading typical timescales [*Kamide and Kokubun*, 1996; *Consolini and De Michelis*, 2005] and also with typical timescales involved in the nonlinear response of the Earth's magnetosphere [*Tsurutani et al.*, 1990]. Furthermore, the smaller MI maximum value for *SYM-H* could be due to the effect that internal processes (like loading-unloading ones taking place in the central plasma sheet of the magnetotail region) play on the enhancement of the Earth's ring current. We remind that part of the Earth's ring current enhancement during geomagnetic storms is due to high-latitude ionospheric ion species (typically oxygen O^+) outflowing as a consequence of FAC activation [*Daglis et al.*, 1994].

The observed absence of coupling (direct inference) between Earth's magnetospheric short timescales and the corresponding solar wind ones supports the inherent difficulties in forecasting high-latitude geomagnetic disturbances, as monitored by auroral electrojet index *AE*, using artificial neural networks based on IMF and solar wind parameters at timescales shorter than 1 h [*Pallocchia et al.*, 2007]. The fluctuations at these timescales, although triggered by the transfer of external energy, mass, and momentum, are not mainly directly coupled to the solar wind parameter fluctuations but result from a complex interplay of external and internal processes. Consequently, a better forecasting of processes occurring on fast timescales requires to

find a valid proxy of the internal magnetosphere dynamical state, with a special attention to the state of the Earth's magnetotail plasma sheet. These can be useful for Space Weather prediction models.

In conclusion, our analysis of relevant coupling timescales during geomagnetic storms and substorms by using both EMD and DMI methods evidenced additional aspects of the solar wind-magnetosphere coupling because (i) a nonstationary and nonlinear analysis can be carried out by using the EMD without any a priori assumptions on the decomposition basis (as for less novel techniques), (ii) the scale-to-scale DMI analysis shows a quantitative evidence of the existence of a timescale separation in solar wind-magnetosphere coupling, and (iii) differently from linear cross-correlation analysis, the DMI performs total linear and nonlinear correlation analysis.

Appendix A: Effect of Propagation From L1 to Bow Shock Nose

A1. OMNI-Based Propagation Method

One way to study solar wind properties at the bow shock nose position is to use the OMNI database. The shift procedure is based on single spacecraft measurements made by ACE and WIND, shifted by assuming that solar wind variations are organized in series of phase fronts, convecting with the solar wind bulk speed. In this way, the time shift equation is

$$\delta t = \frac{\vec{n} \cdot \left(\vec{R}_d - \vec{R}_o\right)}{\vec{n} \cdot \vec{V}} \tag{A1}$$

where $\vec{n}$ is the variation phase front normal (PFN), $\vec{R}_d$ is the bow shock position, $\vec{R}_o$ is the spacecraft position (L1), and $\vec{V}$ is the solar wind velocity. To determine normals to discontinuity planes in the solar wind magnetic field, a modified version of the minimum variance analysis (MVA) technique is used (see *Weimer et al.* [2003], *Bargatze et al.* [2005], *Haaland et al.* [2006], and *Weimer and King* [2008], for more details). The MVA is only applied on magnetic field data, although the location of the bow shock nose $\vec{R}_d$ requires the knowledge of other solar wind parameters such as velocity, proton and alpha particle densities, proton temperature, and ram pressure. Indeed, it is assumed that the geocentric direction to the bow shock nose is parallel to the solar wind flow direction (a correction is needed to take into account mean orbital speed of the Earth around the Sun) such that

$$|\vec{R}_d| = R_{\mathrm{mp}} \left[1.0 + 1.1 \frac{\frac{2}{3}M^2 + 2}{\frac{8}{3}(M^2 - 1)}\right] \tag{A2}$$

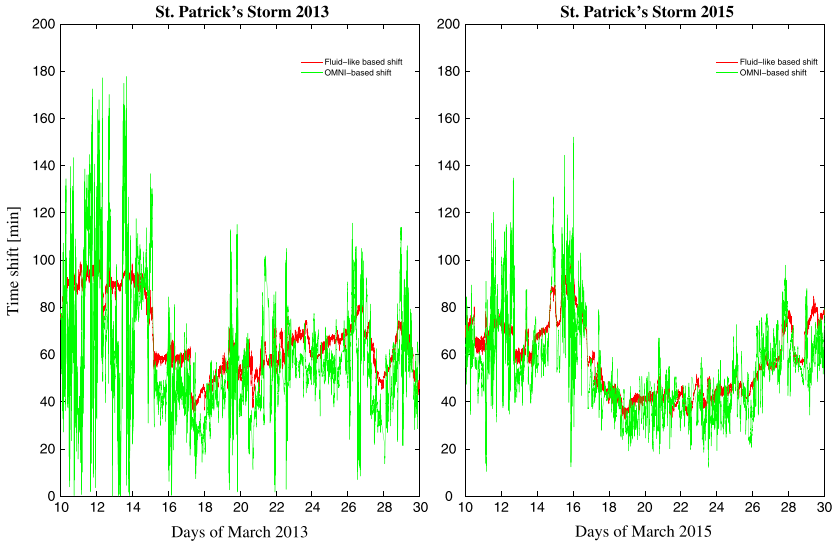

Figure A1. Time shifts obtained with the two different methods described in Appendix A for both St. Patrick's Day storms in 2013 and 2015. Green line refers to the OMNI-based shift procedure as in section A1, while red line shows the time shift obtained via the procedure as in section A2.

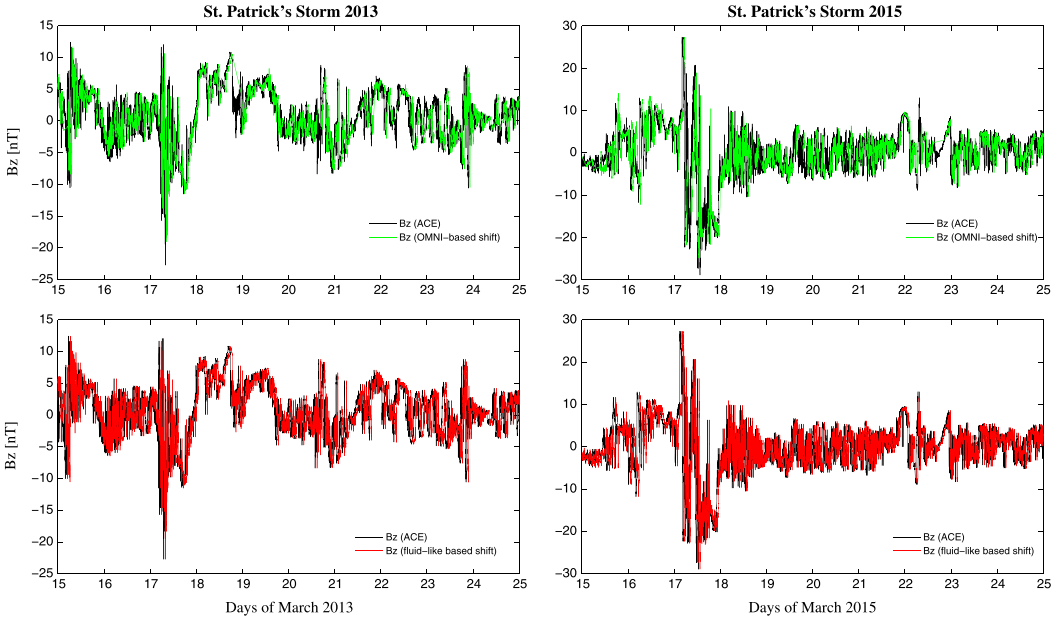

Figure A2. Time behavior of the interplanetary magnetic field B_z component as obtained from raw data by ACE and by using both time shift propagation methods. Black lines refer to the observed values (i.e., ACE data), green lines to OMNI-based time-shifted data and red line to fluid-like based time-shifted data. We zoom over the time interval 15–25 March in both cases for a more convenient visual inspection.

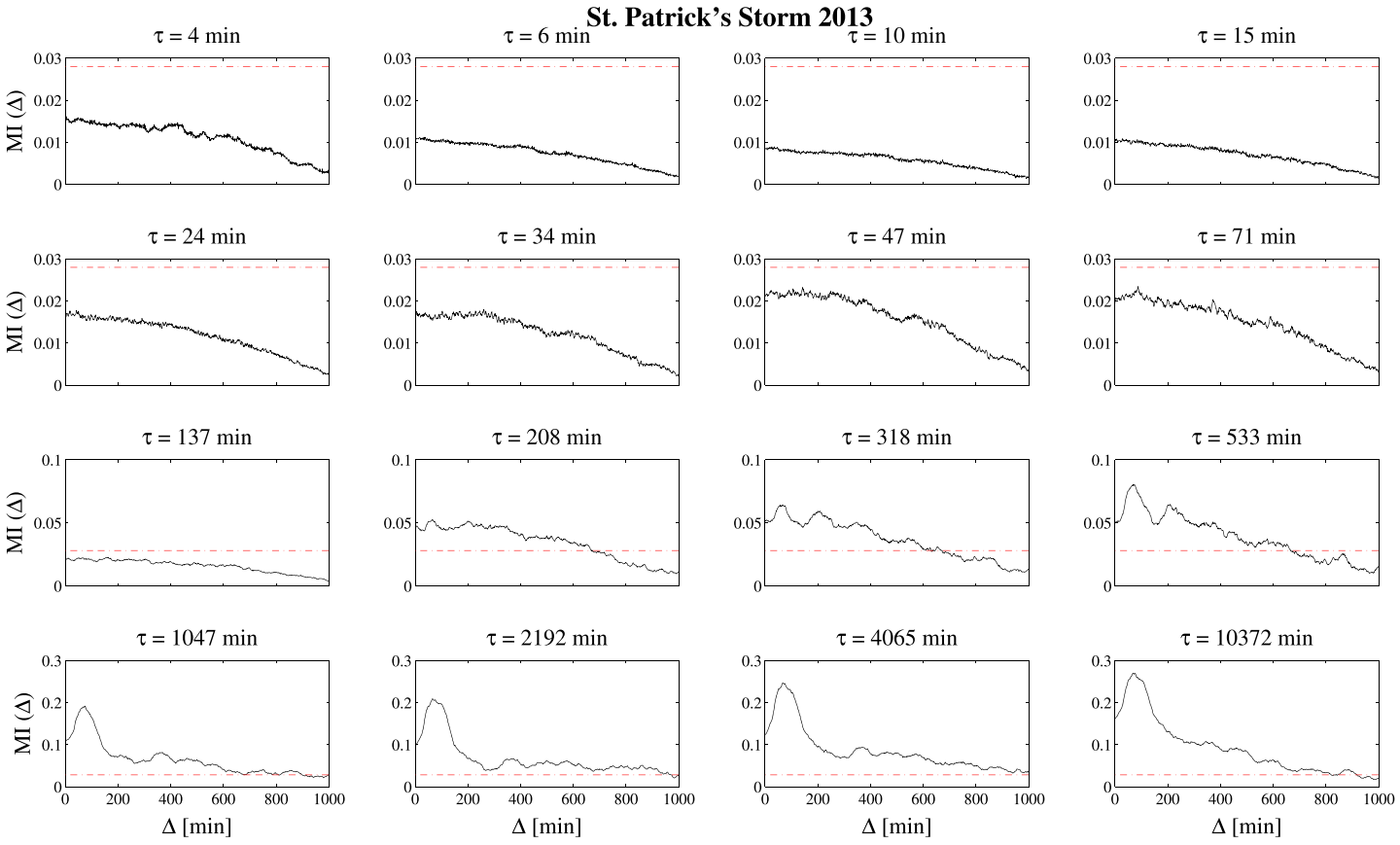

Figure A3. The scale-to-scale DMI between IMFs of the fluid-like based shifted ACE B_z component and auroral electroject *AE* index for the St. Patrick's storm 2013 time period. Red dashed line indicates the significance (5% null hypothesis) DMI threshold, $MI_{thr} = 0.028$.

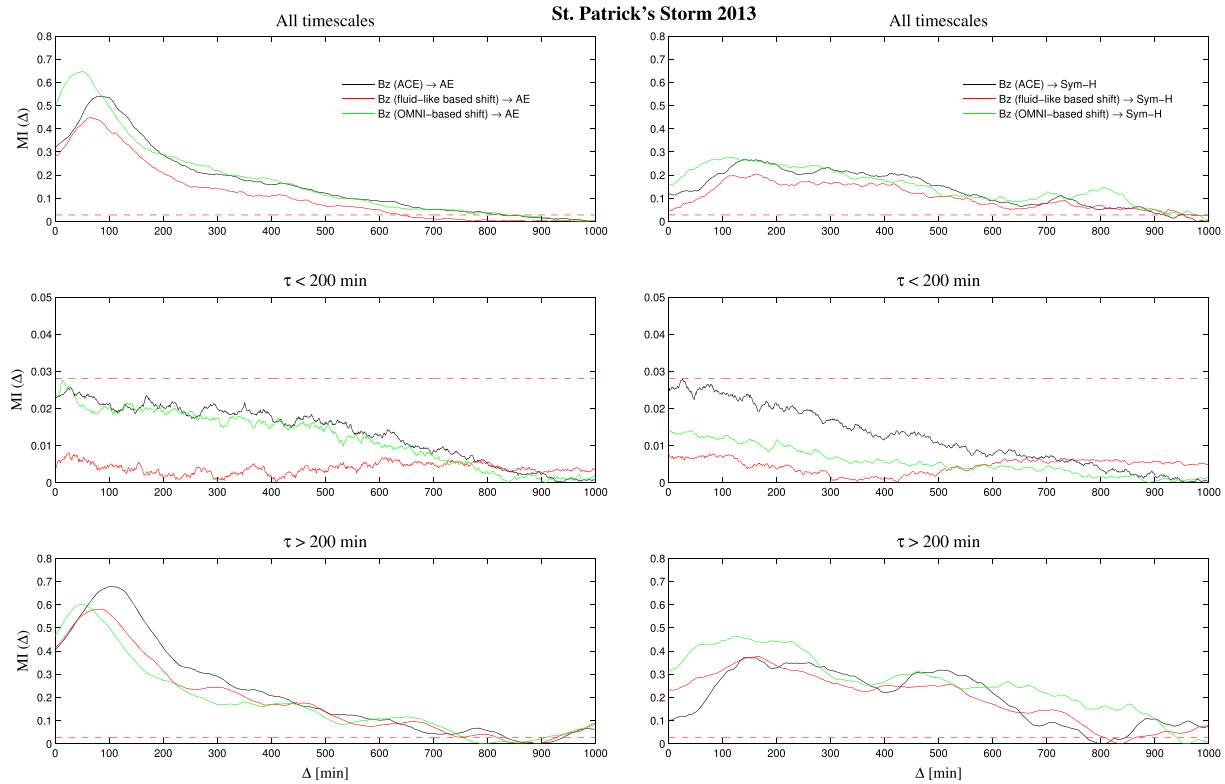

Figure A4. The DMI analysis between IMFs of the interplanetary magnetic field B_z component and auroral electroject *AE* index for (top row) the actual, (middle row) the short-timescale ($\tau < 200$ min), and (bottom row) the long-timescale ($\tau > 200$ min) signals for the 2013 St. Patrick's storm time period. Black line is related to the DMI applied by using observed value of B_z by ACE, while green and red lines refer to the different time shift methods used. The dashed red line is the significance (5% null hypothesis) DMI threshold, $\mathrm{MI}_{\mathrm{thr}} = 0.028$.

with

$$M = \frac{V_{\mathrm{sw}}}{V_{\mathrm{ms}}} \tag{A3}$$

$$V_{\mathrm{ms}} = \sqrt{0.5\left\{V_A^2 + V_s^2 + \sqrt{\left[\left(V_A^2 + V_S^2\right)^2 + 4(V_A^2 V_S^2 \cos^2(\theta)\right]}\right\}} \tag{A4}$$

$$V_A = \frac{B}{\sqrt{4\pi(4N_a + N_p)M_p}} \tag{A5}$$

$$V_s = 0.12\sqrt{T_p + 1.28 \times 10^5} \tag{A6}$$

$$R_{\mathrm{mp}} = (11.4 + KB_z)P^{-1/6.6} \tag{A7}$$

$$P = (2 \times 10^{-6})N_p V_p^2 \tag{A8}$$

where R_{mp} is the geocentric magnetopause nose distance, M is the magnetosonic Mach number, V_{ms} is the magnetosonic speed, V_A is the Alfven speed, V_S is the sound speed, θ is the angle between $\vec{B}$ and $\vec{v}$, N_a and N_p are the alpha particle and proton densities, M_p is the proton mass, T_p is the proton temperature, V_p is the proton velocity, and P is the pressure.

Nevertheless, the time shift procedure is built up by making a "rigid" time shift between the L1 and the nose of the bow shock positions that does not consider the "real" solar wind structure propagation. Indeed, solar wind streams can interact and generate new types of structures which cannot be simply monitored by "rigidly" shifting solar wind parameter values. As also pointed out by OMNI documentation

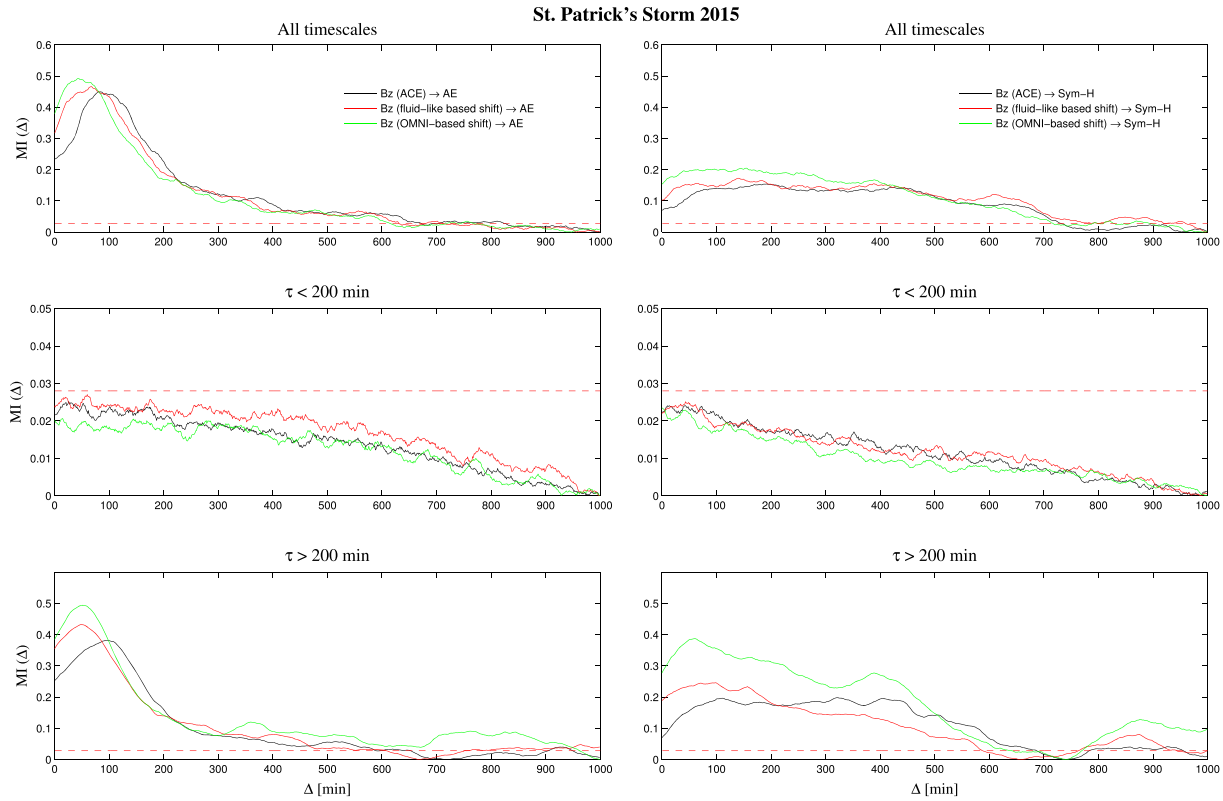

Figure A5. As in Figure A4 for the 2015 St. Patrick's storm time period.

(http://omniweb.gsfc.nasa.gov/html/HROdocum.html) their time shift technique "is a very simplified approach, neglecting finite response times of the magnetosphere to solar wind variations, that may introduce some errors." Additional details about OMNI procedure can be found at http://omniweb.gsfc.nasa.gov/html/HROdocum.html.

A2. Fluid-Like Based Propagation Method

We try to propagate, in a "fluid" sense, different from the "wave-like" propagation made by OMNI (by using shock front direction), ACE spacecraft data. We built up a procedure characterized by the following steps: (i) we identified the direction of the relative positions of ACE spacecraft and bow shock nose ($\vec{r}$), (ii) we projected the solar wind velocity vector measured by ACE ($\vec{v}$) on that direction, and (iii) we evaluate the corresponding time shift as

$$\tau_s = \frac{|\vec{r}|}{\vec{v} \cdot \vec{r}} \tag{A9}$$

where $\vec{r} = \vec{R}_d - \vec{R}_o$ in which the bow shock nose position $\vec{R}_d$ is calculated as in equation (A2). Similarly to the OMNI shifting procedure, we used "Level 2" 16 s magnetic field data and 64 s plasma data obtained by ACE to evaluate both the location of the bow shock nose $\vec{R}_d$ and the "fluid-like" time shift (equation (A9)). Then, we applied the same procedure developed by OMNI to shift time series, i.e., by changing their time tags and resampling time series at 1 min. As for the OMNI procedure, our approach is based on "rigid" time shift, without any consideration of the "in situ" solar wind structure generation. Indeed, the solar wind is a complex system in which several processes can develop and the bow shock surface is not "static" but it is continuously modified by the solar wind itself. This problem could be solved by making the necessary time shift, which implies a complete knowledge of the solar wind properties at L1 position and, simultaneously, the bow shock properties, including magnetic field topology and geometry (this cannot be correctly done since only two satellites are present at L1 and a "topological and geometrical view" of solar wind structures is not possible). Moreover, we should also know the properties of the heliospheric medium between L1 and the bow shock nose positions, since, as stated above, several structures can be generated "in situ" due to solar wind streams interaction and a correct estimation of their formation is not possible by only using spacecraft data

from L1 position. A solution of this problem could be found if we had a numerical model for the bow shock position and also for each solar wind structure in order to investigate its evolution in the heliospheric medium between L1 and bow shock nose positions.

A3. Effect on DMI Analysis

Using the two methods described in the previous sections, we have computed the time shifts for the two geomagnetic storms under consideration. The obtained time shifts for both St. Patrick's Day storms in 2013 and 2015, which are shown in Figure A1, allow us to reconstruct propagated (time shifted) signals (see Figure A2) to which we can apply all the same analysis described in the text to compute the DMI.

Similarly to Figure 5, Figure A3 shows the scale-to-scale DMI in the case of the IMFs relative to the fluid-like shifted B_z component and the *AE* index for the 2013 St. Patrick's Day storm. This analysis confirms that for timescales $\tau < 200$ min the coupling is not significant, while at timescales $\tau \gtrsim 200$ min the coupling becomes significant for time delays Δ in the range $\Delta \in [0, \sim 600-800)$ min, with a maximum of the DMI for a delay $\Delta \sim 60-70$ min.

Moving from these observations, in Figures A4 and A5 we report the results of the DMI analysis between B_z and *AE* or *SYM-H* for the 2013 and 2015 St. Patricks's storms, respectively. The results clearly show the following:

1. A reduction of the time delay Δ from $\sim 100-150$ min to $\sim 70-80$ min. The observed time delay for propagated data is well in agreement with what was generally reported in the literature [see, e.g., *Lyons et al.*, 1997].
2. The absence of a significative correlation at timescales shorter than 200 min, which confirms the previous results on the meaningfulness of DMI at these timescales.
3. An increase of the value of the DMI maximum value for OMNI-based shifted data when all the timescales are considered. This is generally true also at timescales larger than 200 min.

The same results have been found also for the other interplanetary quantities considered in this work.

Acknowledgments

This research work is partly supported by the Italian MIUR-PRIN grant 2012P2HRCR on *The active Sun and its effects on Space and Earth climate*, and by Space Weather Italian Community (SWICO) Research Program. The authors acknowledge J.H. King and N. Papatashvilli at NASA and CDA Web for solar wind data. Acknowledgments are also due to N. Ness of Bartol Research Institute, PI of ACE magnetic field instrument, and to D.J. McComas of Southwest Research Institute, PI of ACE/SWEPAM Solar Wind Experiment. The OMNI data were obtained from the GSFC/SPDF OMNIWeb interface at http://omniweb.gsfc.nasa.gov. The authors also acknowledge World Data Center for Geomagnetism (Kyoto) for the use of the geomagnetic indices data. The EMD code used for the analysis was developed by A. Vecchio. All the derived data products presented in this paper are available upon request by email to the authors (tommaso.alberti@unical.it).

References

Ahn, B. H., S. I. Akasofu, and Y. Kamide (1983), The Joule heat production rate and the particle energy injection rate as a function of the geomagnetic indices *AE* and *AL*, *J. Geophys. Res.*, *88*, 6275–6287.

Akasofu, S. I. (1983), Solar-wind disturbances and the solar wind-magnetosphere energy coupling function, *Space Sci. Rev.*, *34*, 173–183.

Alberti, T., F. Lepreti, A. Vecchio, E. Bevacqua, V. Capparelli, and V. Carbone (2014), Natural periodicities and Northern Hemisphere-Southern Hemisphere connection of fast temperature changes during the last glacial period: EPICA and NGRIP revisited, *Clim. Past*, *10*, 1751–1762, doi:10.5194/cp-10-1751-2014.

Alberti, T., M. Piersanti, A. Vecchio, P. De Michelis, F. Lepreti, V. Carbone, and L. Primavera (2016), Identification of the different magnetic field contributions during a geomagnetic storm in magnetospheric and ground observations, *Ann. Geophys.*, *34*, 1069–1084, doi:10.5194/angeo-34-1069-2016.

Bargatze, L. F., R. L. McPherron, J. Minamora, and D. Weimer (2005), A new interpretation of Weimer et al's solar wind propagation delay technique, *J. Geophys. Res.*, *110*, A07105, doi:10.1029/2004JA010902.

Consolini, G. (1997), Sandpile cellular automata and the magnetospheric dynamics, in *Cosmic Physics in the Year 2000, Proceedings of 8th GIFCO Conference*, vol. 58, edited by S. Aiello et al., pp. 123–126, SIF, Bologna, Italy.

Consolini, G. (2002), Self-organized criticality: A new paradigm for the magnetotail dynamics, *Fractals*, *10*, 275–283.

Consolini, G., and T. S. Chang (2001), Magnetic field topology and criticality in geotail dynamics: Relevance to substorm phenomena, *Space Sci. Rev.*, *95*, 309–321.

Consolini, G., and P. De Michelis (2005), Local intermittency measure analysis of *AE* index: The directly driven and unloading component, *Geophys. Res. Lett.*, *32*, L05101, doi:10.1029/2004GL022063.

Consolini, G., and P. De Michelis (2011), Rank ordering multifractal analysis of the auroral electroject index, *Nonlinear Processes Geophys.*, *18*, 277–285.

Consolini, G., and P. De Michelis (2014), Permutation entropy analysis of complex magnetospheric dynamics, *J. Atmos. Sol. Terr. Phys.*, *115–116*, 25–31, doi:10.1016/j.jastp.2013.11.005.

Consolini, G., M. F. Marcucci, and M. Candidi (1996), Multifractal structure of auroral electroject index data, *Phys. Rev. Lett.*, *76*, 4082–4085.

Consolini, G., P. De Michelis, and R. Tozzi (2008), On the Earth's magnetospheric dynamics: Nonequilibrium evolution and the fluctuation theorem, *J. Geophys. Res.*, *113*, A08222, doi:10.1029/2008JA013074.

Clauer, C. R., and R. L. McPherron (1980), The relative importance of the interplanetary electric field and magnetospheric substorms on partial ring current development, *J. Geophys. Res.*, *85*, 6747–6759.

Clauer, C. R., R. L. McPherron, and C. Searles (1983), Solar wind control of the low latitude asymmetric magnetic disturbance field, *J. Geophys. Res.*, *88*, 2123–2130.

Crooker, N. C. (1972), High-time resolution of the low-latitude asymmetric disturbance in the geomagnetic field, *J. Geophys. Res.*, *77*, 773–775.

Crooker, N. C., and G. L. Siscoe (1971), A study of geomagnetic disturbance field asymmetry, *Radio Sci.*, *6*, 495–501.

Daglis, L. A., S. Livi, E. T. Sarris, and B. Wilken (1994), Energy density of ionospheric and solar wind origin ions in the near-Earth magnetotail during substorms, *J. Geophys. Res.*, *99*, 5691–5703.

Davies, T. N., and M. Sugiura (1966), Auroral electrojet activity index *AE* and its universal time variations, *J. Geophys. Res.*, *71*, 785–801.

De Michelis, P., and G. Consolini (2015), On the local Hurst exponent of geomagnetic field fluctuations: Spatial distribution for different geomagnetic activity levels, *J. Geophys. Res. Space Physics*, *120*, 2691–2701, doi:10.1002/2014JA020685.

De Michelis, P., G. Consolini, M. Materassi, and R. Tozzi (2011), An information theory approach to the storm-substorm relationship, *J. Geophys. Res.*, *116*, A08225, doi:10.1029/2011JA016535.
De Michelis, P., G. Consolini, and R. Tozzi (2012), On the multi-scale nature of large geomagnetic storms: An empirical mode decomposition analysis, *Nonlinear Process Geophys.*, *19*, 667–673.
De Michelis, P., G. Consolini, and R. Tozzi (2015), Latitudinal dependence of short timescale fluctations during intense geomagnetic storms: A permutation entropy approach, *J. Geophys. Res. Space Physics*, *120*, 5633–5644, doi:10.1002/2015JA021279.
Finch, I., and M. Lockwood (2007), Solar wind-magnetosphere coupling functions on timescales of 1 day to 1 year, *Ann. Geophys.*, *25*, 495–506.
Haaland, S., G. Paschmann, and B. U. Ö. Sonnerup (2006), Comment on "A new interpretation of Weimer et al's solar wind propagation delay technique" by Bargatze et al., *J. Geophys. Res.*, *111*, A06102, doi:10.1029/2005JA011376.
Huang, N. E., Z. Shen, S. R. Long, M. L. C. Wu, H. H. Shih, Q. N. Zheng, N. C. Yen, C. C. Tung, and H. H. Liu (1998), The empirical mode decomposition and the Hilbert spectrum for nonlinear and non-stationary time series analysis, *Proc. R. Soc. A*, *454*, 903–995.
Kamide, Y., and S. Kokubun (1996), Two-component auroral electrojet: Importance for substorm studies, *J. Geophys. Res.*, *101*, 13,027–13,046.
Kan, J. R., and L. C. Lee (1979), Energy coupling function and solar wind-magnetosphere dynamo, *Geophys. Res. Lett.*, *6*, 577–580.
Kawasaki, K., and S.-I. Akasofu (1971), Low latitude DS component of geomagnetic storm field, *J. Geophys. Res.*, *76*, 2396–2405.
Klimas, A. J., D. Vassiliadis, N. Baker, and D. A. Roberts (1996), The organized nonlinear dynamics of the magnetosphere, *J. Geophys. Res.*, *101*, 13,089–13,113.
Kovacs, P., V. Carbone, and Z. Voros (2001), Wavelet-based filtering of intermittent events from geomagnetic time-series, *Planet. Space Sci.*, *49*(12), 1219–1231.
Laurenza, M., A. Vecchio, M. Storini, and V. Carbone (2012), Quasi-biennial modulation of galactic cosmic rays, *Astrophys. J.*, *749*, 167.
Lyons, L. R., G. T. Blanchard, J. C. Samson, R. P. Lepping, T. Yamamoto, and T. Moretto (1997), Coordinated observations demonstrating external substorm triggering, *J. Geophys. Res.*, *102*, 27,039–27,051.
Merrill, R. T., M. W. McElhinny, and P. L McFadden (1996), *The Magnetic Fields of the Earth: Paleomagnetism, the Core and the Deep Mantle*, Academic Press, San Diego, Calif.
Newell, P. T., T. Sotirelis, K. Liou, C.-I. Meng, and F. J. Rich (2007), A nearly universal solar wind-magnetosphere coupling function inferred from 10 magnetospheric state variables, *J. Geophys. Res.*, *112*, A01206, doi:10.1029/2006JA012015.
Pallocchia, G., E. Amata, G. Consolini, M. F. Marcucci, and I. Bertello (2007), *AE* index forecast at different time scales through an ANN algorithm based on L1 IMF and plasma measurements, *J. Atmos. Sol. Terr. Phys.*, *70*, 663–668.
Perreault, P., and S.-I. Akasofu (1978), A study of geomagnetic storms, *Geophys. J. R. Astron. Soc.*, *54*, 547–573.
Rostoker, G., J. A. Vallance, R. L. Gattinger, C. D. Anger, and J. S. Murphree (1987), The development of the substorm expansive phase: The "eye" of the substorm, *Geophys. Res. Lett.*, *14*, 399–405.
Shannon, C. E. (1948), A mathematical theory of communication, *Bell Syst. Tech. J.*, *27*, 379–423.
Sharma, A. S. (1995), Assessing the magnetosphere's nonlinear behavior: Its dimension is low, its predictability, high, *Rev. Geophys.*, *33*, 645–650.
Sitnov, M. I., S. Sharma, K. Papdopoulos, and D. Vassiliadis (2001), Modeling substorm dynamics of the magnetosphere: From self-organization and self-organized criticality to nonequilibrium phase transitions, *Phys. Rev. E*, *65*, 16116.
Sugiura, M., and D. J. Poros (1971), Hourly values of equatorial *Dst* for years 1957 to 1970, Rep. X-645-71-278, 1971, Goddard Space Flight Cent., Greenbelt, Md.
Tsurutani, B., M. Sugiura, T. Iyemori, B. E. Goldstein, W. D. Gonzalez, S. I. Akasofu, and E. J. Smith (1990), The nonlinear response of *AE* to the IMF B_s, *Geophys. Res. Lett.*, *17*, 279–282.
Tsurutani, B. T., R. Hajra, E. Echer, and J. W. Gjerloev (2015), Extremely intense (SML ≤ -2500 nT) substorms: Isolated events that are externally triggered?, *Ann. Geophys.*, *33*, 519–524, doi:10.5194/angeo-33-519-2015.
Uritsky, V. M., and M. I. Pudovkin (1998), Low frequency $1/f$-like fluctuations of the *AE*-index as a possible manifestation of self-organized criticality in the magnetosphere, *Ann. Geophys.*, *16*, 1580–1588.
Uritsky, V. M., A. J. Klimas, D. Vassiliadis, D. Chua, and G. Parks (2002), Scale-free statistics of spatiotemporal auroral emissions as depicted by POLAR UVI images: The dynamics magnetosphere is an avalanching system, *J. Geophys. Res.*, *107*(A12), 1426.
Vassiliadis, D. (2006), System theory for geospace plasma dynamics, *Rev. Geophys.*, *44*, RG2002, doi:10.1029/2004RG000161.
Vecchio, A., M. Laurenza, V. Carbone, and M. Storini (2010a), Quasi-biennal modulation of solar neutrino flux and galactic cosmic rays by solar cyclic activity, *Astrophys. J. Lett.*, *709*, L1–L5.
Vecchio, A., V. Capparelli, and V Carbone (2010b), The complex dynamics of the seasonal component of USA's surface temperature, *Atmos. Chem. Phys.*, *10*, 9657–9665.
Vecchio, A., M. Anzidei, V. Capparelli, V. Carbone, and I. Guerra (2012a), Has the Mediterranean Sea felt the March 11th, 2011, M_w 9.0 Tohoku-Oki earthquake?, *Europhys. Lett.*, *98*, 59001.
Vecchio, A., M. Laurenza, D. Meduri, V. Carbone, and M. Storini (2012b), The dynamics of the solar magnetic field: Polarity reversals, butterfly diagram, and quasi-biennial oscillations, *Astrophys. J.*, *749*, 27.
Vecchio, A., F. Lepreti, M. Laurenza, T. Alberti, and V. Carbone (2017), Connection between solar activity cycles and grand minima generation, *Astron. Astrophys.*, *599*, A58, doi:10.1051/0004-6361/201629758.
Wanliss, J. A. (2005), Fractal properties of *SYM-H* during quiet and active times, *J. Geophys. Res.*, *110*, A03202, doi:10.1029/2004JA010544.
Wanliss, J. A., and V. Uritsky (2010), Understanding bursty behavior in midlatitude geomagnetic activity, *J. Geophys. Res.*, *115*, L04107, doi:10.1029/2009JA014642.
Weimer, D. R., and J. H. King (2008), Improved calculations of interplanetary magnetic field phase front angles and propagation time delays, *J. Geophys. Res.*, *113*, A01105, doi:10.1029/2007JA012452.
Weimer, D. R., D. M. Ober, N. C. Maynard, M. R. Collier, D. J. McComas, N. F. Ness, C. W. Smith, and J. Watermann (2003), Predicting interplanetary magnetic field (IMF) propagation delay times using the minimum variance delay technique, *J. Geophys. Res.*, *108*(A1), 1026, doi:10.1029/2002JA009405.
Wu, Z., and N. E. Huang (2004), A study of the characteristics of white noise using the empirical mode decomposition method, *Proc. R. Soc. A*, *460*, 1597–1611.